NANO LETTERS

Letter

pubs.acs.org/NanoLett

Engineering the Size Distributions of Ordered GaAs Nanowires on Silicon

Jelena Vukajlovic-Plestina,[†,⊥] Wonjong Kim,[†,⊥] Vladimir G. Dubrovski,[‡,§,∥,⊥] Gözde Tütüncüoğlu,[†] Maxime Lagier,[†] Heidi Potts,[†] Martin Friedl,[†] and Anna Fontcuberta i Morral*[,†]

[†]Laboratoire des Matériaux Semiconducteurs, École Polytechnique Fédérale de Lausanne, 1015 Lausanne, Switzerland

[‡]St. Petersburg Academic University, Khlopina 8/3, 194021 St. Petersburg, Russia

[§]Ioffe Physical Technical Institute of the Russian Academy of Sciences, Politekhnicheskaya 26, 194021 St. Petersburg, Russia

[∥]ITMO University, Kronverkskiy pr. 49, 197101 St. Petersburg, Russia

Supporting Information

ABSTRACT: Reproducible integration of III−V semiconductors on silicon can open new path toward CMOS compatible optoelectronics and novel design schemes in next generation solar cells. Ordered arrays of nanowires could accomplish this task, provided they are obtained in high yield and uniformity. In this work, we provide understanding on the physical factors affecting size uniformity in ordered GaAs arrays grown on silicon. We show that the length and diameter distributions in the initial stage of growth are not much influenced by the Poissonian fluctuation-induced broadening, but rather are determined by the long incubation stage. We also show that the size distributions are consistent with the double exponential shapes typical for macroscopic nucleation with a large critical length after which the nanowires grow irreversibly. The size uniformity is dramatically improved by increasing the As_4 flux, suggesting a new path for obtaining highly uniform arrays of GaAs nanowires on silicon.

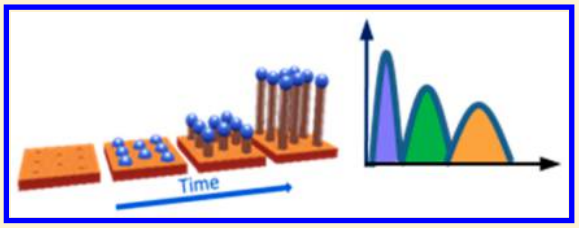

KEYWORDS: *Nanowires, heterogeneous integration, arrays, self-catalyzed, Ga-assisted growth, length distribution, sub-Poissonian statistics*

Semiconductor nanowires (NWs) are filamentary crystals with a tailored diameter ranging between few and ∼100 nm. Their anisotropic morphology and small lateral size result in many interesting properties that are different from bulk materials. NWs have thus inspired a large variety of applications and fundamental studies, such as miniaturized optoelectronics,[1−3] next generation energy harvesting,[4,5] quantum communication, and computing.[6] Very importantly, small footprint in contact with the substrate allows for facile strain relaxation in heteroepitaxy, enabling defect-free growth of NWs on lattice-mismatched substrates. This has opened the path for monolithic integration of high performance III−V materials with Si electronic platform.

Obtaining NWs in predefined positions constitutes the first step toward their utilization as devices in scalable platforms. Electronics, optoelectronics, and energy harvesting require a clear outline of the device structure on a chip.[5,7−12] In addition, in a bottom-up growth process, the structure of NW arrays can be extremely dependent on the interwire distance and the initial conditions such as the droplet size.[13−16] Preparing growth initiation in predefined sites is essential for understanding the fundamental aspects of the entire NW growth process that can otherwise be hidden in a self-assembly process. Only with this comprehension, we will reproducibly engineer the NW morphology and dimensions and thus promote their further transfer from laboratory to industry.

NWs are usually obtained by the bottom-up vapor−liquid−solid (VLS) method, in which a liquid metal droplet directs the NW growth. One of the approaches to fabricate ordered arrays of NWs relies upon the positioning of lithographically defined nanoscale droplets. Gold, the most used metal in VLS, should be avoided in any silicon platform with electronic or optoelectronic functionality.[17,18] Instead, self-catalyzed growth has arisen as a reliable alternative to gold-assisted VLS growth. In the case of GaAs, gallium droplets can also initiate and direct the growth of GaAs NWs. In order to obtain growth in predefined sites, nanoscale holes are created in a dielectric layer. Gallium is then selectively deposited into the holes, thereby initiating NW growth in these sites.[19,20] GaAs NW arrays on silicon substrates have been achieved by few groups, although yields close to 100% are rare.[20−23] Achieving a yield close to 100% is key for a real integration of III-Vs on silicon. Achieving such high yield necessitates a very thorough understanding of both the initial stages of growth (wetting of the Ga droplet and nucleation mechanisms) and the nanowire elongation. In this work, with the base of having achieved a yield close to 90% we focus on the latter. To the best of our knowledge, fundamental studies of the initial stages of NW nucleation and growth and in

Received: February 27, 2017
Revised: May 24, 2017
Published: June 14, 2017

DOI: 10.1021/acs.nanolett.7b00842
Nano Lett. 2017, 17, 4101−4108

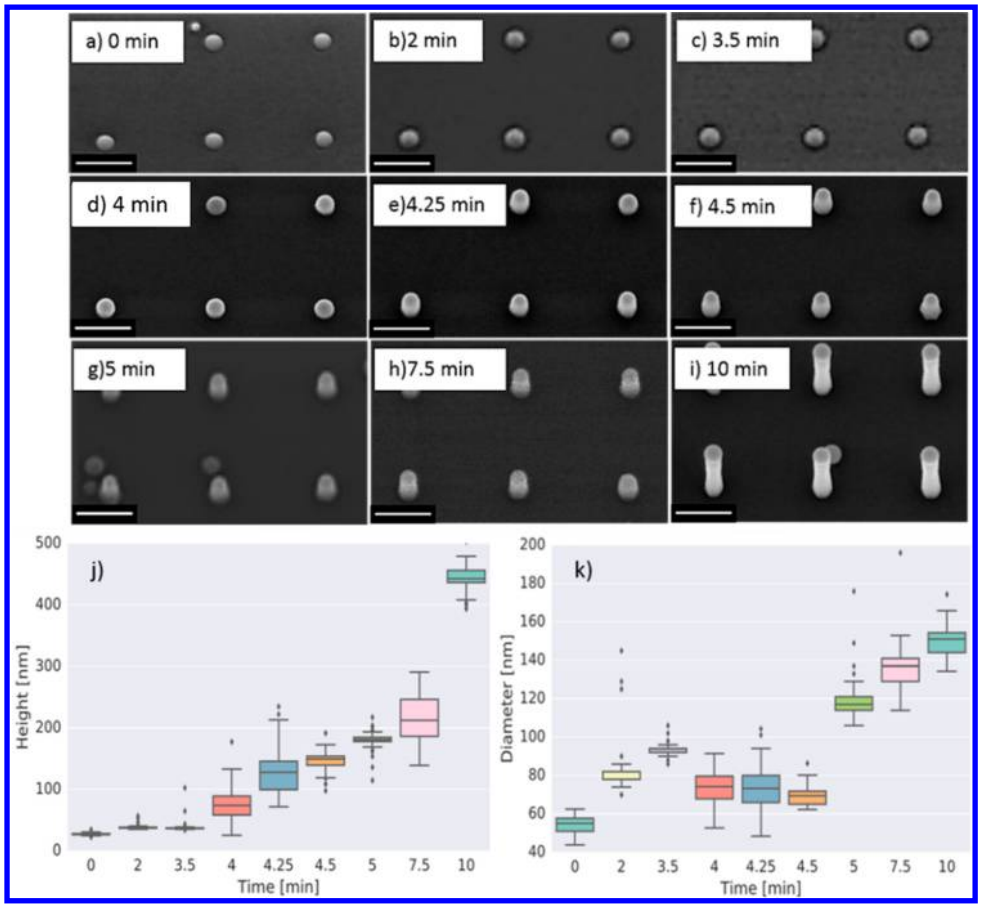

Figure 1. Time series of GaAs NW arrays: (a–i) SEM images of the array grown for from 0 min (droplet deposition) up to 10 min. The scale bar is 200 nm, and tilt angle is 20°; corresponding height (j) and diameter (k) distributions obtained by AFM. Far field SEM images showing the homogeneity of the whole array can be found in SI.

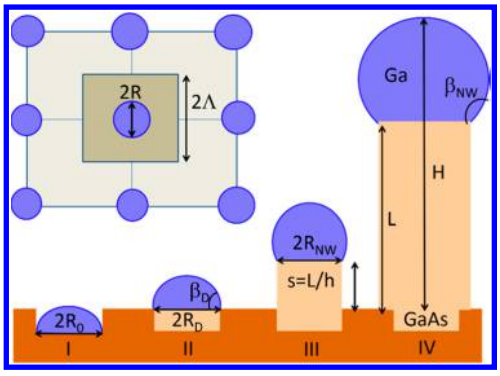

Figure 2. Proposed scheme of Ga-catalyzed VLS growth of GaAs NWs in regular arrays: I, droplet predeposition (t = 0); II, formation of the initial NW monolayers after the incubation phase (t > 0); III, initial elongation of the NW and IV definition of the NW morphological parameters.

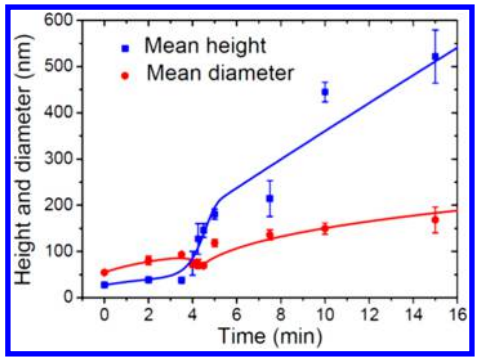

Figure 3. Mean NW height H(including the droplet height) and top diameter $2R$ versus time (symbols) for GaAs NWs grown from holes of 45 nm nominal diameter (due to the HF dip, the actual hole size at the beginning of gallium deposition is actually larger, about 60 nm). The growth time of 4 min can be associated with the incubation time of the nanowires. In our modeling, t_* = 4.5 min is the moment corresponding to when most NWs emerge from the substrate. $2\Delta t$ = 1 min is the duration of the incubation stage, which is approximately symmetrical around the maximum. Therefore, the nucleation of NWs effectively starts after $t_* - \Delta t$ = 4 min. The error bars represent standard deviation. The curves show best fits obtained from the model equations.

particular the influence of the incubation time on the resulting length and diameter distributions within the NW ensembles in ordered arrays are still lacking.

Recently, it was predicted theoretically[24−26] and confirmed experimentally[24] that Ga-assisted GaAs NWs may exhibit narrow diameter distribution under optimized conditions. Theoretical studies also showed that the NW length distribution can be narrowed with respect to Poissonian by a nucleation antibunching process,[27−29] but only in the absence of delay for NW nucleation on the surface.[30] Unfortunately, a sub-Poissonian length distribution has never been observed in NW ensembles. This applies for both Au-catalyzed and self-catalyzed VLS NWs as well as non-VLS NWs grown by selective area epitaxy on in the self-induced approach. A careful

DOI: 10.1021/acs.nanolett.7b00842
Nano Lett. 2017, 17, 4101−4108

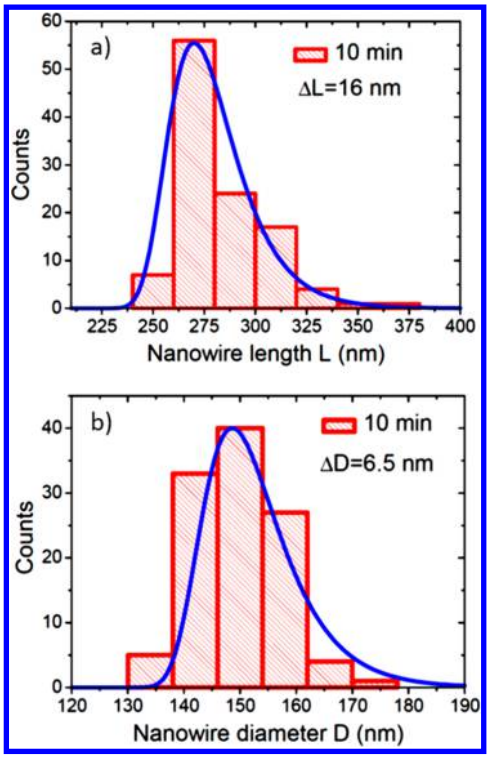

Figure 4. (a) Length histogram of Ga-catalyzed GaAs NWs after 10 min of growth (without droplets), fitted by the double exponential distribution with ΔL = 16 nm. (b) Diameter histogram of Ga-catalyzed GaAs NWs after 10 min of growth, fitted by the double exponential distribution with ΔD = 6.5 nm.

study on the NW length distributions necessitates a frame that guarantees that each NW grows under the same conditions and starts at the same time. Here, for the first time, we present the size (length and diameter) distributions of Ga-assisted GaAs NWs grown in the ordered arrays on Si. The high yield obtained allows us to reliable derive a model on the evolution of the NW elongation and diameter with time. Overall, this study opens a new avenue for the deterministic integration of III−V nanowires on silicon.

Results and Discussion. We start by illustrating the initial stages of GaAs NW growth on patterned silicon substrate. The growth is performed on a (111)Si substrate covered with a 10 nm thick thermal oxide, in which we etch nanoscale holes with reactive ion etching (details on substrate fabrication and design can be found in the Methods section and SI 1). The yield of vertical NWs was higher than 85%. Figure 1a−i shows the typical scanning electron micrographs (SEM) of GaAs NW arrays obtained on 45 nm wide holes as a function of time. For this series of samples, we used the gallium flux corresponding to the GaAs growth rate of 1 Å/s, the As_4 partial pressure of 2×10^{-6} Torr (unless indicated otherwise), at a substrate temperature of 635°.

Wide field SEM pictures of the arrays showing the consistent yield across a 100 × 100 μm^2 area are shown in SI 2. The high and uniform yield can only be achieved with a 10 min Ga predeposition step, denoted as growth time of 0 min in Figure 1a. The SEM images present the NW morphology evolution after the intervals of 2, 3.5, 4, 4.25, 4.5, 5, 7.5, and 10 min in Figure 1b−i, respectively. Here, the images for each time interval are all taken from newly grown samples and not from resumed growth. The measurement of the elongation statistics on newly grown samples is justified here because of the extremely high reproducibility of the samples. Samples obtained under the same conditions lead to identical statistical results. If instead one would restart growth from the same sample, one would expect to achieve less relevant results as the oxidation of the GaAs nanowire and Ga droplet could perturb the reinitiation of growth. In order to follow more precisely the initial stages of growth, we have performed the atomic force microscopy (AFM) analysis of the same area. The average height and diameter of the nanostructures versus time are given in Figure Figure 1j,k, along with the corresponding statistical data for the size distributions for each point. These data were acquired by measuring at least 125 NWs for each sample. The data are illustrated in the line−box plots, where 50% of the distribution is within the box and the horizontal band inside corresponds to the statistical median of the distribution. The bottom and the top of the line include 98% of the distribution, while the points outside of the line correspond to the measurements that fall farther from the main distribution.

The NW growth does not start right after the Ga predeposition. Rather, we observe a delay of 3.5 min under these growth conditions. The delay is detected in both the SEM micrographs and in the height evolution as plotted in Figure 1j. After 4 min of growth, we detect an increase in height and a sudden decrease in the diameter. The mean NW height increases very rapidly and the length distribution broadens once the NWs start emerging from the substrate. This effect is well-understood because increasing the number density of NWs that start at different time necessarily leads an enlargement of the distribution width. A similar long nucleation step has been previously reported for a variety of systems, including Au-catalyzed InAs NWs,[24] In-catalyzed InAs NWs, and Ga-catalyzed GaAs NWs grown without any gallium predeposition.[25]

We now turn to modeling the initial stages of NW growth in regular arrays. Figure 2 illustrates the parameters that are used to describe the evolution of NW height and diameter. Initially, the gallium droplets exhibit a radius R_0 at the base, which can be smaller than or equal to that of the hole. The contact angle of the droplets resting on the surface is denoted β_D and should be close to 90° (See SI3). During the incubation stage, most droplets just swell on the surface by increasing their base radius R_D without changing much their contact angle, while almost no NWs start.

The NW nucleation requires that the droplet is lifted up to a certain macroscopic value of the height. In our model we use the dimensionless length $s = L/h \gg 1$ Figure 2a-III) (with h = 0.326 nm as the height of GaAs monolayer). The NW initiation process is expected to exhibit a barrier activated character and proceed via macroscopic nucleation. This means that the critical length s_c, i.e., the length after which the NWs begin to grow regularly in vertical direction and at a fixed contact angle of the droplets on their tops, is much larger than unity. After growth has started ($s > s_c$), the droplets acquire the contact angle β_{NW} which is larger than β_D. This abrupt change of the droplet shape leads to the corresponding decrease of the droplet base radius. The total height of the structures (droplets and NWs) equals $H = L + R(1 - \cos\beta)/\sin\beta$, where L is the NW length excluding the droplet, R is the droplet base radius, and β is the contact angle. The volume of spherical cap droplet is given by $V = (\pi R^3/3)f(\beta) = i\Omega_{Ga}$. Here, i is the number of gallium atoms in spherical cap (we neglect the influence of arsenic on the droplet volume due to its low concentration,[32]

DOI: 10.1021/acs.nanolett.7b00842
Nano Lett. 2017, 17, 4101−4108

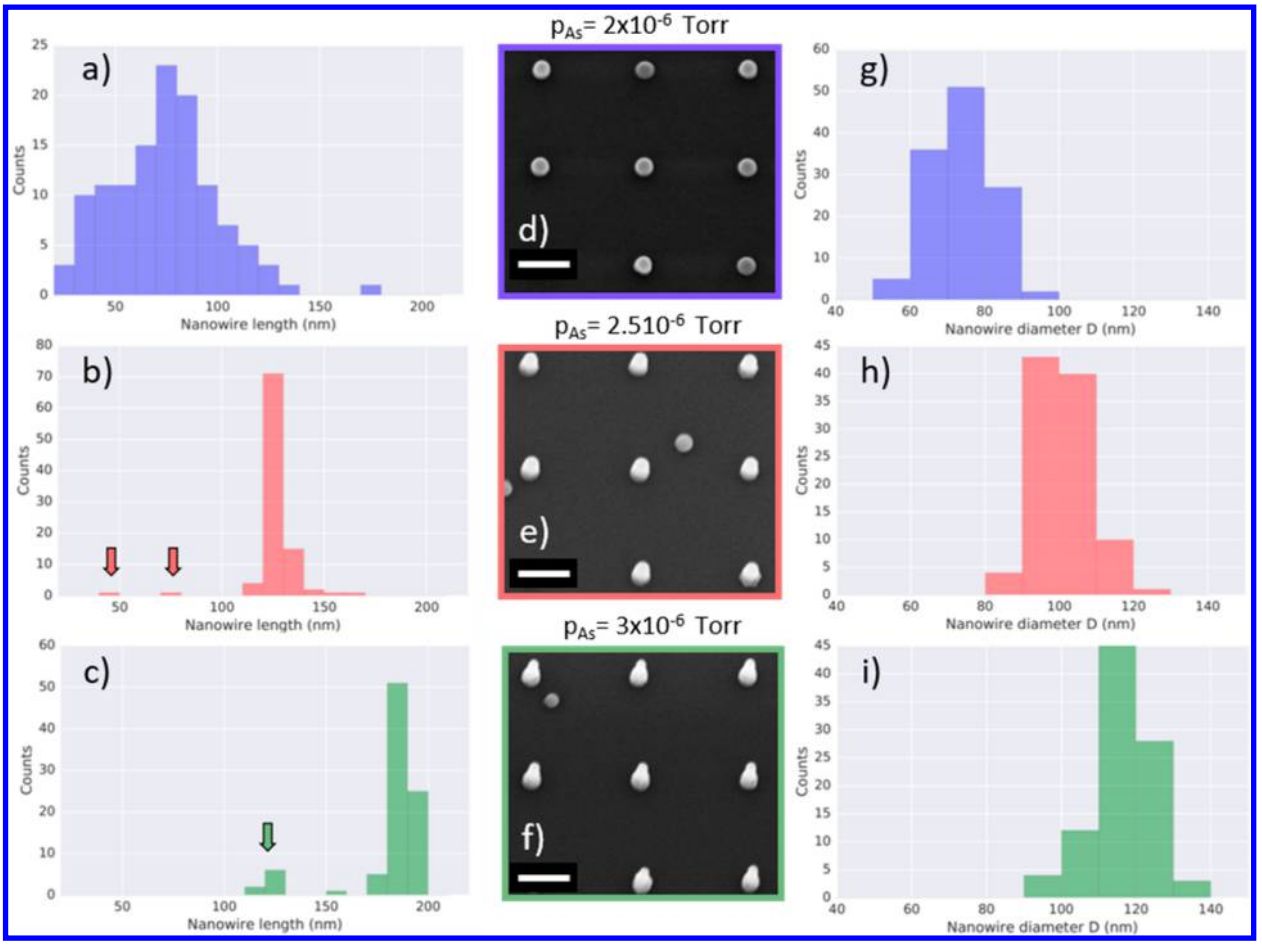

Figure 5. As series grown for 4 min. (a–c) NW length distributions for As pressure 2 × 10^{-6}, 2.5 × 10^{-6}, and 3 × 10^{-6} Torr, respectively, (d–f) Corresponding SEM micrographs. The scale bar is 200 nm, and the tilt angle 20°. (g–i) NW diameter distributions. The effect of As pressure is evident in terms of higher growth rates and narrowing the distributions, particularly for the NW length.

Ω_{Ga} = 0.02 nm^3 is the elementary volume of liquid gallium, and $f(\beta) = (1 - \cos\beta)(2 + \cos\beta)/[(1 + \cos\beta)\sin\beta]$ is the geometrical function relating the volume of spherical cap to the cube of its base. The droplet base radius is related to i as $R = R_{Ga}(\beta)_i^{1/3}$, with $R_{Ga}(\beta) = [3\Omega_{Ga}/(\pi f(\beta))]^{1/3}$ being the shape-dependent characteristic size.

We start the modeling of the growth process by relating the material conservation with the model geometry shown in Figure 2. If we assume that all gallium atoms impinging onto different surfaces will subsequently reach the droplet,[33] the number of gallium atoms in the droplet changes in time according to[27]

$$\frac{di}{dt} = \frac{\nu_{Ga}}{\Omega_{GaAs}}\left[(4\Lambda^2 - \pi R^2)\cos\alpha_{Ga} + 2RL\sin\alpha_{Ga} + \frac{\pi R^2}{\sin^2\beta}\right] - \frac{\pi R^2}{\Omega_{GaAs}}\frac{dL}{dt} \quad (1)$$

Here, ν_{Ga} = 6.6 nm/min is the gallium rate in our conditions and Ω_{GaAs} = 0.0452 nm^3 is the elementary volume of solid GaAs. The first term in the right-hand side of eq 1 stands for the gallium collection from the surface area per NW, with 2Λ ≅ 400 nm as the array pitch and α_{Ga} = 45° as the incident angle of the gallium beam. The second term describes the atoms collected by the NW sidewalls, the third gives the number of gallium atoms collected by the droplet, and the fourth is the sink due to the NW axial growth. In the first approximation, the axial growth rate is proportional to the effective arsenic influx ν_{As}, including a contribution from re-emitted arsenic species[32,34,35]

$$\frac{dL}{dt} = \chi_{As}\nu_{As} \quad (2)$$

In these conditions, the main contribution to di/dt in eq 1 is given by the size-independent term $(\nu_{Ga}/\Omega_{GaAs})4\Lambda^2\cos\alpha_{Ga}$, explaining why we observe a pronounced regime of radial growth rather than droplet shrinking or self-stabilization.[34−36] From eqs 1 and 2, the "invariant" variables for which the growth rates are size-independent are given by the number of gallium atoms in the droplet and the number of GaAs monolayers in the NW:[33]

$$\frac{di}{dt} = \frac{1}{\tau}, \quad \frac{ds}{dt} = \frac{1}{\tau_s} \quad (3)$$

The time $\tau \cong \Omega_{GaAs}/(4\Lambda^2\nu_{Ga}\cos\alpha_{Ga})$ with our parameters is estimated at 1.5 × 10^{-8} min. The time $\tau_s = h/(\chi_{As}\nu_{As})$ approximately equals 0.012 min (the $\chi_{As}\nu_{As}$value approximately equals 28 nm/min, and it is determined by fitting the data as will be discussed shortly). Equation 3 for di/dt applies for droplets as well as NWs. Integrating it, we obtain the base radius in the form

DOI: 10.1021/acs.nanolett.7b00842
Nano Lett. 2017, 17, 4101−4108

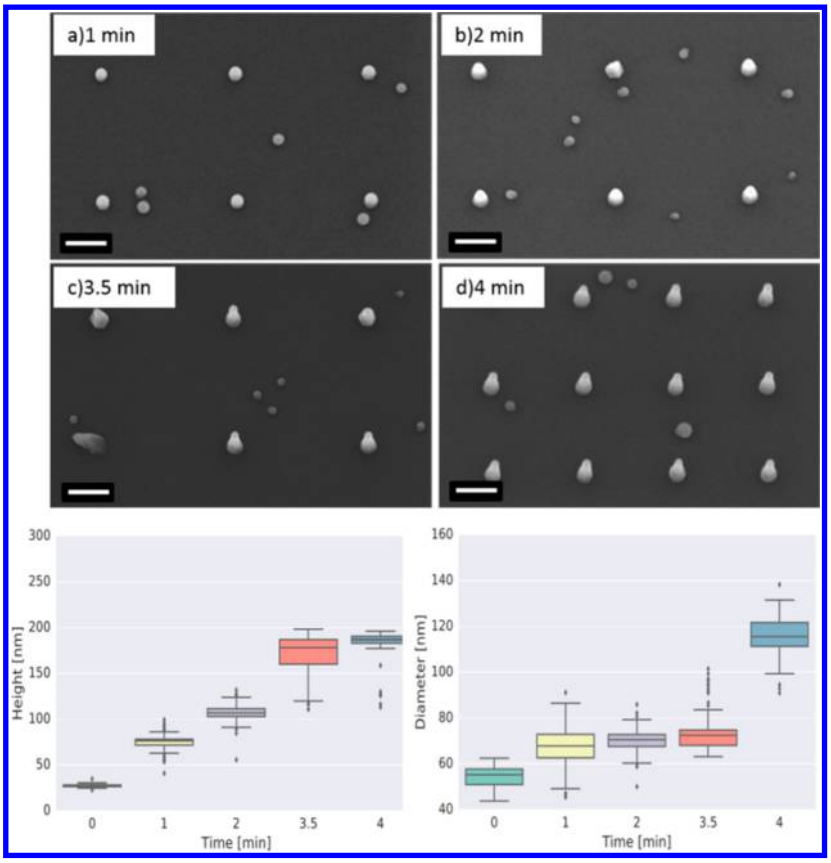

Figure 6. Time series for 3×10^{-6} Torr. (a–d) SEM images of the arrays grown for different times, (e) height distributions, and (f) diameter distributions as a function of time. Spurious growth on the oxide occurs occasionally, and it is attributed to the presence of defects on the oxide surface. We have not detected any effect of the presence of these droplets on the overall nanowire yield and/or time evolution. Far field SEM images showing the homogeneity of the whole array can be found in the SI.

$$R_D = \left[{R_0}^3 + {R_{Ga}}^3(\beta_D)\frac{t}{\tau} \right]^{1/3} \tag{4}$$

The droplet height is obtained simply by using the total height of the structure, H, with R_D given by eq 4, and setting $L = 0$ by the droplet definition:

$$H_D = R_D \frac{(1 - \cos \beta_D)}{\sin \beta_D} \tag{5}$$

Here, β_D is the contact angle of the droplets resting on the surface. Assuming that the transformation from droplets to NWs occurs at a fixed volume of liquid gallium, the radius and height of NWs are given by

$$R_{NW} = \left[\frac{f(\beta_0)}{f(\beta_{NW})} \right]^{1/3} R_D$$

$$H_{NW} = \chi_{As} v_{As} t + R_{NW} \frac{(1 - \cos \beta_{NW})}{\sin \beta_{NW}} \tag{6}$$

where β_{NW} is the contact angle of the droplets seated at the NW tops.

Our goal now is to understand the evolution of NW array as an ensemble. The NW ensemble evolves from droplets to NWs, passing through an initial stage where there is coexistence of droplets and NWs. Consequently, the description of radius and height evolution should also include nucleation statistics. The mean radius and height within an ensemble containing both droplets and NWs should be obtained as a weighted average of the two populations. We use macroscopic nucleation theory in open systems to describe the statistical size distributions. We define $p_{NW}(t)$ as the normalized number density of NWs. In macroscopic nucleation theory,[28] this $p_{NW}(t)$ is the double exponential function of time

$$p_{NW} = 1 - \exp\left[-\exp\left(\frac{t - t_*}{\Delta t} \right) \right] \tag{7}$$

Here, t_* is moment of time corresponding to the maximum nucleation rate of NWs and Δt is the duration of the incubation stage. The NWs that start at time t_* will subsequently correspond to the maximum of the size distributions. The normalized number density of droplets, p_D, corresponds to $p_D(t) = 1 - p_{NW}(t)$. Using these number densities as probabilities to observe either a droplet or NW in a given site, the mean radius and height of the structures (denoted $\langle R \rangle$ and $\langle H \rangle$, respectively) are obtained as

$$\langle R \rangle = R_D p_D + R_{NW} p_{NW}$$

$$\langle H \rangle = H_D p_D + H_{NW} p_{NW} \tag{8}$$

These expressions describe a competition between the two populations of droplets and nanowires throughout the incubation stage and the follow-up nucleation stage within the time interval $0 \le t \le t_c = t_* + \Delta t$. At $t > t_c$, the population of droplets diminishes to zero and the NWs continue growing with the mean radius and height given by

DOI: 10.1021/acs.nanolett.7b00842
Nano Lett. 2017, 17, 4101–4108

$$\langle R\rangle = \left[\langle R\rangle_c^{\,3} + R_{Ga}^{\,3}(\beta_{NW})\frac{a(t-t_c)}{\tau}\right]^{1/3}$$

$$\langle H\rangle = \langle L\rangle_c + b\chi_{As}\nu_{As}(t-t_c) + \langle R\rangle\frac{(1-\cos\beta_{NW})}{\sin\beta_{NW}} \quad (9)$$

Here, the a and b factors describe possible differences in the material supply to longer NWs. Best fits of the mean diameter and height as a function of time following eqs 8 and 9 are shown in Figure 3. They were obtained with β_{NW} 130°, $t_* = 4.5$ min, $\Delta t = 0.5$ min, $\tau = 6 \times 10^{-8}$ min, $\chi_5\nu_5 = 28$ nm/min, $a = 14$, and $b = 1$.

Let us now discuss the choice of the model parameters. The contact angle of the droplet sitting on the NW top is set to its typical value during growth.[26] We set $b = 1$, ignoring any difference between the NW elongation rate at the initial and steady state growth stages. The times t_* and Δt are determined from our experimental data. As mentioned above, $t_* = 4.5$ min is the time moment corresponding to the maximum nucleation of NWs emerging from the substrate and $2\Delta t = 1$ min the duration of the incubation stage, which is approximately symmetrical around the maximum. Therefore, the nucleation of NWs effectively starts after $t_* - \Delta t = 4$ min. We thus deduce an incubation time of 4 min in these growth conditions, which corresponds to the NW nucleation delay due to difficult emerging from the substrate. The fitting value of $\tau = 6 \times 10^{-8}$ min is close to that obtained earlier from geometrical considerations (1.5×10^{-8} min). The obtained value $\chi_5\nu_5$ of 28 nm/min appears reasonable, in agreement with an atomic V/III flux ratio of 4.2. The value of $a = 14$ implies that droplets receive a larger gallium influx in the steady state stage with respect to the beginning of growth. This can be due to re-emission or additional contributions of gallium adatoms diffusing from the NW sidewalls, the terms that were omitted in material balance given by eq 1.

We now move to modeling the NW size distributions. According to refs 36−40, whenever the number density of NWs is given by eq 7, there will be a broadening of the size distributions for both lengths and diameters in the initial stage of growth, simply because the distribution width increases from initially zero to its final value where the nucleation stage is completed. In the steady-state growth stage, the size distributions can be further broadened due to kinetic fluctuations. These Poissonian contributions to the broadening should contribute less than 5% for our short growth times (see SI 4). As a consequence, we ignore the effect of kinetic fluctuations in our model. The width of the resulting length distributions are now mostly determined by the incubation stage. The equations used to fit our experimental size distributions for the 10 min growth were the following:

$$f(L, L_*) = A\exp\left[\frac{L_* - L}{\Delta L} - \exp\left(\frac{L_* - L}{\Delta L}\right)\right] \quad (10)$$

for the NW lengths without the droplet, with L_* as the most representative length and $\Delta L = \chi_{As}\nu_{As}\Delta t$ as the distribution width. Note that here we consider the NW length without droplets, that is, $L = H - H_D$. For the diameter distribution, we use the similar expression

$$f(R, R_*) = CR^2\exp\left[\frac{R_* - R}{\Delta R} - \exp\left(\frac{R_* - R}{\Delta R}\right)\right] \quad (11)$$

with the width $\Delta R = R_{Ga}^{\,3}(\beta_D)\Delta t/(3R_*^{\,2}\tau)$. Details of derivation of these expressions are given in SI 4. The length and diameter histograms of NWs after 10 min of growth are shown in Figure 4, along with their best fits by the double exponential shapes given by eqs 10 and 11. With our parameters, the calculated values of the distribution widths equal $\Delta L = 14$ nm, $2\Delta R = 4.5$ nm (see SI 4), while from the fits they are 16 and 6.5 nm, respectively.

While obtaining a high yield of GaAs arrays is relevant for the integration of III-Vs on silicon, it would be even more important to obtain the most homogeneous size distribution possible. This brought us to explore the conditions that could further narrow the length and radius distributions of NWs. So far, our model indicates that the length distributions are primarily determined by the incubation stage, i.e., different start times for the regular VLS growth of different NWs. In order to achieve more uniform arrays, we increased As_4 beam flux. Our intention was to achieve a higher supersaturation in the Ga droplet and thus increase the GaAs nucleation probability,[37,38] or to decrease the nucleation time Δt, which primarily determines the width of the length and diameter distributions. This should shorten the incubation time for NW growth and hence the decrease the initial size distribution width. We compare the elongation and diameter distributions of NWs obtained after 4 min of growth since this corresponds to the incubation time for NWs obtained at lowest As_4 fluxes. We show results for As_4 equivalent beam pressures of 2×10^{-6}, 2.5×10^{-6}, and 3×10^{-6} Torr in Figure 5. We include both the SEM micrographs and the corresponding size distributions. As expected, by increasing the As_4 flux both the NW incubation phase and the nucleation step shorten. The length distribution width is also considerably narrowed. The mean values for lengths are (75 ± 25), (125 ± 12), and (180 ± 10) nm, for histograms in Figure 5a−c, respectively. From the values of standard deviations, one can observe that the distribution narrows for more the factor 2 when As pressure was increased from 2×10^{-6} Torr to value of 3×10^{-6} Torr. These results confirm that increasing supersaturation in the Ga droplets is a good strategy for increasing the NW homogeneity in the arrays.

The values indicated with arrows in Figure 5b,c are probably the wires for which droplets were consumed or polycrystalline material (unsuccessful nucleation of NW). These features cannot be distinguished solely from AFM scans. In SI 4, we have also looked at the time evolution of NW growth under the highest supersaturation conditions. Figure 6a−d depicts representative SEM micrographs and the statistical morphological analysis as a function of the growth time. The incubation time of the NWs is shorter than 1 min. This represents a factor of 4 in reduction of the incubation period by just a 50% an increase in the As_4 equivalent beam flux pressure. This confirms the strong nonlinear relation between nucleation statistics and supersaturation.

Conclusions. In conclusion, we have provided a detailed study of the initial stages of growth of ordered GaAs NWs on silicon. The NW nucleation leads to a rapid shape transformation of droplets in which their base radius shrinks and the height increases accordingly. Our NWs grow under strongly gallium-rich conditions corresponding to the droplet swelling. The widths of both radius and length distributions do not follow Poissonian fluctuation-induced broadening for the short lengths investigated, but rather are determined by the long nucleation stage. Interestingly, our statistical histograms do not show any pronounced asymmetry toward longer left tails, as in

DOI: 10.1021/acs.nanolett.7b00842
Nano Lett. 2017, 17, 4101−4108

refs 30 and 31. Instead, they are well-fitted by the double exponential shapes typical for macroscopic nucleation with a large critical length after which NWs grow irreversibly. Our model describe well the observed distribution shapes; however, unraveling the exact mechanisms of NWs emerging from the substrate requires a separate study. Shortening the nucleation stage by increasing the As_4 flux effectively narrows the size distribution. Our results suggest that this parameter plays a key role for obtaining uniform arrays on silicon. In addition, we believe that these results apply to other VLS growth using low surface energy metals such as Sn/Ga-catalyzed GaP NWs or Sn/In-catalyzed InAs NWs.

Methods. *Substrate Preparation.* Four-inch ⟨111⟩ p-doped silicon wafers with a resistivity of 0.1−0.5 Ω·cm; 10 nm were thermally oxidized in a Centrotherm furnace at 950 °C. The thickness of silicon oxide was 15 nm. The pattern was predefined in a ZEP resist with electron-beam lithography and then transferred on the oxide layer by a 6 s dry etching using CHF_3/SF_6 chemistry followed by 2 s dip in 7:1 buffered hydrofluoric acid solution (BHF). Electron-beam resist was removed by oxygen plasma. After patterning, the wafers were diced into 35 × 35 mm^2 square chips sized for the MBE sample holder. In order to ensure an oxide-free surface in the holes, the chips were shortly dipped in the same BHF solution prior to the introduction in the UHV chamber. The final thickness of oxide before loading was 10 ± 1 nm. The substrates were subsequently annealed at 500 °C for 2 h in UHV in order to ensure a pristine surface free of water and organic molecules. The substrate was then transferred to the growth chamber. There, they were degassed at 770 °C for 30 min to further remove any possible surface contaminants.

■ ASSOCIATED CONTENT

Supporting Information

The Supporting Information is available free of charge on the ACS Publications website at DOI: 10.1021/acs.nanolett.7b00842.

Substrate design, SEM images of the high yield samples, details on the contact angle of Ga, complete derivation of the model used here, and details on how the length distributions are experimentally obtained (PDF)

■ AUTHOR INFORMATION

Corresponding Author

*E-mail: anna.fontcuberta-morral@epfl.ch.

ORCID

Vladimir G. Dubrovski: 0000-0003-2088-7158

Anna Fontcuberta i Morral: 0000-0002-5070-2196

Author Contributions

⊥The first three authors contributed equally.

Notes

The authors declare no competing financial interest.

■ ACKNOWLEDGMENTS

Authors thank the following funding agencies for their support: FP9 Nanoembrace, H2020 Indeed, SNF through ERANET-Russia project nr IZLRZ2_163861, the NCCR QSIT, and MPI-EPFL center. W.K. thanks the Blaise Pascal Excellence Scholarship. J.V.P. thanks CMI for access to the nanofabrication and characterization facilities. V.G.D. gratefully acknowledges financial support received from the Ministry of Education and Science of the Russian Federation under grant 14.613.21.0055 (project ID: RFMEFI61316X0055).

■ REFERENCES

(1) Joyce, H. J.; et al. III − V semiconductor nanowires for optoelectronic device applications. *Prog. Quantum Electron.* **2011**, *35*, 23−75.

(2) Bessire, C. D.; et al. Trap-Assisted Tunneling in Si-InAs Nanowire Heterojunction Tunnel Diodes. *Nano Lett.* **2011**, *11*, 4195−4199.

(3) Li, Y.; Qian, F.; Xiang, J.; Lieber, C. M. Nanowire electronic and optoelectronic devices Electronic and optoelectronic devices impact many areas of society. *Mater. Today* **2006**, *9*, 18−27.

(4) Krogstrup, P.; et al. Single-nanowire solar cells beyond the Shockley−Queisser limit. *Nat. Photonics* **2013**, *7*, 306−310.

(5) Tian, B.; et al. Coaxial silicon nanowires as solar cells and nanoelectronic power sources. *Nature* **2007**, *449*, 885−889.

(6) Frolov, S. M.; Plissard, S. R.; Nadj-Perge, S.; Kouwenhoven, L. P.; Bakkers, E. P. a. M. Quantum computing based on semiconductor nanowires. *MRS Bull.* **2013**, *38*, 809−815.

(7) Zhao, Y.; et al. Shape-Controlled Deterministic Assembly of Nanowires. *Nano Lett.* **2016**, *16*, 2644−2650.

(8) Morales, A. M. A Laser Ablation Method for the Synthesis of Crystalline Semiconductor Nanowires. *Science (Washington, DC, U. S.)* **1998**, *279*, 208−211.

(9) Zhou, W.; Dai, X.; Lieber, C. M. Advances in nanowire bioelectronics. *Rep. Prog. Phys.* **2017**, *80*, 16701.

(10) Gudiksen, M. S.; Lauhon, L. J.; Wang, J.; Smith, D. C.; Lieber, C. M. Growth of nanowire superlattice structures for nanoscale photonics and electronics. *Nature* **2002**, *415*, 617−620.

(11) Huang, Y.; Xiangfeng Duan, Q.; Wei, C. M. L. Directed Assembly of One-Dimensional Nanostructures into Functional Networks. *Science* **2001**, *291*, 630−633.

(12) Cui, Y.; Lieber, C. M. Functional nanoscale electronic devices assembled using silicon nanowire building blocks. *Science* **2001**, *291*, 851−3.

(13) Wang, J.; et al. Reversible switching of InP nanowire growth direction by catalyst engineering. *Nano Lett.* **2013**, *13*, 3802−3806.

(14) Jensen, L. E.; et al. Role of surface diffusion in chemical beam epitaxy of InAs nanowires. *Nano Lett.* **2004**, *4*, 1961−1964.

(15) Hertenberger, S. Growth kinetics in position-controlled and catalyst-free InAs nanowire arrays on Si(111) grown by selective area molecular beam epitaxy. *J. Appl. Phys.* **2010**, *108*, 114316.

(16) Borgström, M. T.; Immink, G.; Ketelaars, B.; Algra, R.; Bakkers, E. P. a M. Synergetic nanowire growth. *Nat. Nanotechnol.* **2007**, *2*, 541−544.

(17) Zardo, I.; et al. Growth study of indium-catalyzed silicon nanowires by plasma enhanced chemical vapor deposition. *Appl. Phys. A: Mater. Sci. Process.* **2010**, *100*, 287−296.

(18) Zardo, I.; et al. Gallium assisted plasma enhanced chemical vapor deposition of silicon nanowires. *Nanotechnology* **2009**, *20*, 155602.

(19) Bauer, B.; et al. Position controlled self-catalyzed growth of GaAs nanowires by molecular beam epitaxy. *Nanotechnology* **2010**, *21*, 435601.

(20) Plissard, S.; Larrieu, G.; Wallart, X.; Caroff, P. High yield of self-catalyzed GaAs nanowire arrays grown on silicon via gallium droplet positioning. *Nanotechnology* **2011**, *22*, 275602.

(21) Lee, K. D.; Heidari, B.; van Helvoort, A. T. J.; Fimland, B. O.; Weman, H. Position-Controlled Uniform GaAs Nanowires on Silicon using Nanoimprint Lithography. *Nano Lett.* **2014**, *14*, 960.

(22) Russo-Averchi, E.; et al. High Yield of GaAs Nanowire Arrays on Si Mediated by the Pinning and Contact Angle of Ga. *Nano Lett.* **2015**, *15*, 2869−2874.

(23) Gibson, S.; Lapierre. Study of rad ial growth in patterned self-catalyzed GaAs nanowire arrays by gas sour c e mole c ular beam epitaxy. Phys. *Phys. Status Solidi RRL* **2013**, *849*, 845−849.

DOI: 10.1021/acs.nanolett.7b00842
Nano Lett. 2017, 17, 4101−4108

(24) Dubrovskii, V. G.; Xu, T.; Díaz Álvarez, A.; Plissard, S. R.; Caroff, P.; Glas, F.; Grandidier, B. Self-Equilibration of the Diameter of Ga-Catalyzed GaAs Nanowires. *Nano Lett.* **2015**, *15*, 5580.
(25) Tersoff, J. Stable Self-Catalyzed Growth of III-V Nanowires. *Nano Lett.* **2015**, *15*, 6609−6613.
(26) Dubrovskii, V. G. Kinetic narrowing of size distribution. *Phys. Rev. B: Condens. Matter Mater. Phys.* **2016**, *93*, 174203.
(27) Glas, F.; Harmand, J. C.; Patriarche, G. Nucleation Antibunching in Catalyst-Assisted Nanowire Growth. *Phys. Rev. Lett.* **2010**, *104*, 135501.
(28) Glas, F. Statistics of sub-Poissonian nucleation in a nanophase. *Phys. Rev. B: Condens. Matter Mater. Phys.* **2014**, *90*, 125406.
(29) Dubrovskii, V. G. Self-regulated pulsed nucleation in catalyzed nanowire growth. *Phys. Rev. B: Condens. Matter Mater. Phys.* **2013**, *87*, 195426.
(30) Dubrovskii, V. G.; Sibirev, N. V.; Berdnikov, Y.; Gomes, U. P.; Ercolani, D.; Zannier, V.; Sorba, L.; et al. Length distributions of Au-catalyzed and In-catalyzed InAs nanowires. *Nanotechnology* **2016**, *27*, 375602.
(31) Matteini, F.; et al. Tailoring the diameter and density of self-catalyzed GaAs nanowires on silicon. *Nanotechnology* **2015**, *26*, 105603.
(32) Glas, F.; Ramdani, M. R.; Patriarche, G.; Harmand, J. C. Predictive modeling of self-catalyzed III-V nanowire growth. *Phys. Rev. B: Condens. Matter Mater. Phys.* **2013**, *88*, 195304.
(33) Plante, M. C.; Lapierre, R. R. Analytical description of the metal-assisted growth of III-V nanowires: Axial and radial growths. *J. Appl. Phys.* **2009**, *105*, 114304.
(34) Colombo, C.; Spirkoska, D.; Frimmer, M.; Abstreiter, G.; Fontcuberta I Morral, A. Ga-assisted catalyst-free growth mechanism of GaAs nanowires by molecular beam epitaxy. *Phys. Rev. B: Condens. Matter Mater. Phys.* **2008**, *77*, 155326.
(35) Priante, G.; Ambrosini, S.; Dubrovskii, V. G.; Franciosi, A.; Rubini, S. Stopping and resuming at will the growth of GaAs nanowires. *Cryst. Growth Des.* **2013**, *13*, 3976−3984.
(36) Ramdani, M. R.; Harmand, J. C.; Glas, F.; Patriarche, G.; Travers, L. Arsenic Pathways in Self-Catalyzed Growth of GaAs Nanowires. *Cryst. Growth Des.* **2013**, *13*, 92.
(37) Dubrovskii, V. G. Fluctuation-induced spreading of size distribution in condensation kinetics. *J. Chem. Phys.* **2009**, *131*, 164514.
(38) Dubrovskii, V. G.; Nazarenko, M. V. Nucleation theory beyond the deterministic limit. I. the nucleation stage. *J. Chem. Phys.* **2010**, *132*, 114507.
(39) Dantzig, J. A.; Rappaz, M. *Solidification*, 2th ed.; EPFL Press, 2016.
(40) Ford, I. J. Statistical mechanics of nucleation: a review. *Proc. Inst. Mech. Eng., Part C* **2004**, *218*, 883−899.

DOI: 10.1021/acs.nanolett.7b00842
Nano Lett. 2017, 17, 4101−4108